

Supplementary Material - Stationary shapes of axisymmetric vesicles beyond lowest-energy configurations

Rodrigo B. Reboucas, Hammad A. Faizi, Michael J. Miksis and Petia M. Vlahovska

1 Notes on differential geometry

Let a surface be defined by $\mathbf{x} = \mathbf{x}(u, v)$ in rectangular coordinates, where u, v surface coordinates. Figure 1 shows surface vectors at point P , where the tangent vectors $(\mathbf{x}_u, \mathbf{x}_v)$ span a tangent plane locally and \mathbf{n} is the normal vector given by

$$\mathbf{n} = \frac{\mathbf{x}_u \times \mathbf{x}_v}{|\mathbf{x}_u \times \mathbf{x}_v|} = \frac{\mathbf{x}_u \times \mathbf{x}_v}{\sqrt{EG - F^2}} \quad (1.1)$$

where the direction of the normal depends on the labelling of the coordinate curves. Here, E , F , and G are the coefficients of the first fundamental form in differential geometry [1]

$$E = \mathbf{x}_u \cdot \mathbf{x}_u, \quad F = \mathbf{x}_u \cdot \mathbf{x}_v, \quad G = \mathbf{x}_v \cdot \mathbf{x}_v, \quad (1.2)$$

and hence the differential element of area can be expressed as

$$dA = \sqrt{EG - F^2} du dv, \quad (1.3)$$

where $W = \sqrt{EG - F^2}$ defines a local metric on the surface. The general equation for the mean curvature and Gaussian curvatures are

$$H = \frac{1}{2} \frac{EN - 2FM + GL}{W^2} = \frac{1}{2}(c_1 + c_2), \quad (1.4)$$

and

$$K = \frac{LN - M^2}{W^2} = c_1 c_2, \quad (1.5)$$

where c_1 and c_2 are the principal curvatures, and

$$L = \mathbf{x}_{uu} \cdot \mathbf{n}, \quad M = \mathbf{x}_{uv} \cdot \mathbf{n}, \quad N = \mathbf{x}_{vv} \cdot \mathbf{n}, \quad (1.6)$$

are the coefficients of the second fundamental form. In the case where parametric lines coincide with lines of curvature, the principal curvatures in (1.4) reduce to

$$c_1 = \frac{L}{E}, \quad c_2 = \frac{N}{G}, \quad (1.7)$$

since $F = M = 0$.

It is useful to define the Laplace-Beltrami operator,

$$\Delta_b f = \frac{1}{W} \left(\left(\frac{Ef_v - Ff_u}{W} \right)_v + \left(\frac{Gf_u - Ff_v}{W} \right)_u \right), \quad (1.8)$$

where f is an arbitrary function. For axisymmetric geometries, $F = 0$ and the v -derivatives are set to zero, and hence Eq. (1.8) reduces to

$$\Delta_b f = \frac{1}{W} \left(\frac{G f_u}{W} \right)_u. \quad (1.9)$$

In the general literature on vesicle shapes [2], the metric coefficient g is defined as the determinant of the metric tensor $g_{ij} \equiv \mathbf{x}_i \cdot \mathbf{x}_j$, for $i, j = 1, 2$ such that

$$g_{ij} = \begin{pmatrix} E & F \\ F & G \end{pmatrix}, \quad (1.10)$$

and the curvature tensor $h_{ij} \equiv (\partial_i \partial_j \mathbf{x}) \cdot \mathbf{n}$ is

$$h_{ij} = \begin{pmatrix} L & M \\ M & N \end{pmatrix}. \quad (1.11)$$

Accordingly, the mean curvature in Eq.(1.4) is equivalent to $H \equiv \text{tr}(h_j^i)/2$ where $h_j^i \equiv g^{ik} h_{kj}$ and g^{ik} are the components of the inverse of the metric tensor (1.10), and hence

$$h_j^i = \begin{pmatrix} L/E & 0 \\ 0 & N/G \end{pmatrix}, \quad (1.12)$$

in agreement with Eq. (1.7).

An important distinction between the notation used in standard differential geometry for the mean curvature, \mathbf{H} , and the notation used in the literature on vesicle shape equations, H , is the sign-convention where $H = -\mathbf{H}$. This convention is adopted so that in the limit of a spherical shape, the mean curvature, H , is positive using the standard spherical coordinates notation (i.e., $u = \theta$, and $v = \phi$); see, for instance, the discussion below Eq. (2.9) in Ref. [2].

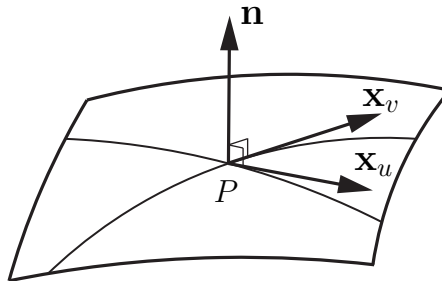


Figure 1: Local representation of the tangent vectors $(\mathbf{x}_u, \mathbf{x}_v)$ at a point P on a surface represented by $\mathbf{x} = \mathbf{x}(u, v)$; outward-pointing normal vector, \mathbf{n} , as indicated.

1.1 Arclength parametrization

The position vector of a point on a axisymmetric surface parameterized by arclength, as shown in Fig.1(b) in the main text, where $u = s$ and $v = \phi$ is

$$\mathbf{x}(s, \phi) = \{r(s) \cos \phi, r(s) \sin \phi, z(s)\}, \quad (1.13)$$

where s is the arclength and ϕ is the azimuthal angle. Using (1.13) in Eq.(1.1) yields the surface normal

$$\mathbf{n}(s, \phi) = \{-z_s \cos \phi, -z_s \sin \phi, r_s\}. \quad (1.14)$$

Using relations (1.13) and (1.14) the coefficients of the first and second fundamental forms reduce to

$$E = 1, \quad F = 0, \quad G = r^2 \quad (1.15)$$

and

$$L = z_{ss}r_s - z_s r_{ss}, \quad M = 0, \quad N = r z_s. \quad (1.16)$$

Using relations in Eq. (1.7) the principal curvatures are given by

$$c_1 = z_{ss}r_s - z_s r_{ss}, \quad (1.17)$$

and

$$c_2 = \frac{z_s}{r}. \quad (1.18)$$

Thus, the mean curvature is completely defined (i.e., $H = -H$), aside from a minus sign depending on the choice of notation. In the arclength parametrization, the Laplace-Beltrami of operator given by (1.9) reduces to

$$\Delta_b f = \frac{1}{r} (r f_s)_s. \quad (1.19)$$

In the tilt-angle formulation discussed in section 2, where $r_s = \cos \psi$ and $z_s = -\sin \psi$, the principal curvatures are

$$c_1 = -\psi_s, \quad (1.20)$$

and

$$c_2 = -\frac{\sin \psi}{r}. \quad (1.21)$$

1.2 Force balance approach

In this section we present a complementary approach to deriving the general shape equation for vesicles following a force balance at the interface. The elastic traction per unit area acting on the membrane can be obtained from

$$\mathbf{f}_m = \frac{\delta^{(1)} E_b}{\delta \mathbf{x}} + \frac{\delta^{(1)} E_\Sigma}{\delta \mathbf{x}}, \quad (1.22)$$

such that

$$\mathbf{f}_m = [-2\kappa \Delta_b H - 4\kappa H(H^2 - K) + 2H\Sigma] \mathbf{n} - \nabla_s \Sigma, \quad (1.23)$$

using the results from Appendix A in the main text and setting $H = -H$. The normal surface traction is discontinuous across the interface and is balanced by internal membrane stresses,

$$\mathbf{n} \cdot [\mathbf{T}_{ex}^h - \mathbf{T}_{in}^h] = \mathbf{f}_m, \quad (1.24)$$

where $T_{ij,k}^h = -p_k \delta_{ij}$ is the second-order, hydrostatic stress tensor and the subscript $k = ex, in$ indicates the exterior and interior regions of the closed vesicle, respectively. Hence,

$$-P \mathbf{n} = \mathbf{f}_m, \quad (1.25)$$

where $P = p_{ex} - p_{in}$, following the definition of pressure difference used in Eq. 8 in the main text. Combining Eqs. (1.25) and (1.23) yields the force balance in the normal direction,

$$2\kappa \Delta_b H + 4\kappa H(H^2 - K) - 2H\Sigma - P = 0 \quad (1.26)$$

in agreement with Eq. (8) in the main text.

2 Tilt-angle formulation for axisymmetric vesicles

The tilt-angle formulation has been extensively used in numerical analyses of stationary shapes of axisymmetric vesicles [2], where the tilt angle ψ is subtended between the tangent vector to the surface and the horizontal direction, as illustrated in Fig. 1(b) of the main text. In this section, we revisit this formulation following the derivation presented in Refs. [3, 4] for completeness of presentation and further comparison with the numerical results shown in sections 3 and 4 in the main text. First, a derivation of the shape equations assuming constant-force ensemble is presented and comments are made about the dynamically equivalent shape equations assuming constant-height.

The general shape equation (8) in the main text can be recast as a system of non-linear ordinary differential equations for axisymmetric vesicles by minimizing the total energy functional Eq. (6). In the tilt-angle approach, the variables $(r, z, \psi; r_s, z_s, \psi_s)$ are taken as independent “coordinates” and “velocites”, where arclength plays the role of time in classical mechanics; thus, the geometric relations between the spatial coordinates (r, z) and the tilt angle

$$r_s = \cos \psi, \quad z_s = -\sin \psi, \quad (2.1)$$

are enforced by Lagrange multipliers (γ, η) , respectively, where $\psi \in [0, \pi]$ for $0 \leq s \leq L$. The total elastic energy (6) in the main text can be written in the terms of a “Lagrangian” function, \mathcal{L} , as follows

$$G'_{\mathcal{L}} = 2\pi\kappa \int_{s_1}^{s_2} \mathcal{L}(r, r_s, z_s, \psi, \psi_s) ds - F\Delta z|_{s=s_1}, \quad (2.2)$$

where s_1 and s_2 are the arclength measures at the north and south poles, respectively, and

$$\mathcal{L} = \frac{r}{2} \left(\psi_s + \frac{\sin \psi}{r} \right)^2 + \frac{\Sigma}{\kappa} r + \frac{1}{2} \frac{P}{\kappa} r^2 \sin \psi + \gamma(r_s - \cos \psi) + \eta(z_s + \sin \psi). \quad (2.3)$$

In Eq. (2.3), the membrane is assumed symmetric and the principal curvatures are given by

$$c_1 = -\psi_s, \quad c_2 = -\frac{\sin \psi}{r}, \quad (2.4)$$

as shown in section 1.1.

Following Halminton’s principle of stationary action derived in section 4 for completeness, where the action functional is given by Eq. (2.2) and the arclength s is treated as time, extrema conditions on the membrane elastic energy are obtained by path variations of the energy functional in the configurational space spanned by the coordinates (r, z, ψ) . Combining Eqs. (4.2) and (4.6), the variation of the elastic energy reduces to

$$\begin{aligned} \frac{\delta G'_{\mathcal{L}}}{2\pi\kappa} = & \int_{s_1}^{s_2} \left\{ \left[\frac{\partial \mathcal{L}}{\partial \psi} - \frac{d}{ds} \frac{\partial \mathcal{L}}{\partial \psi_s} \right] \delta \psi + \left[\frac{\partial \mathcal{L}}{\partial r} - \frac{d}{ds} \frac{\partial \mathcal{L}}{\partial r_s} \right] \delta r \right. \\ & + \left[\frac{\partial \mathcal{L}}{\partial z} - \frac{d}{ds} \frac{\partial \mathcal{L}}{\partial z_s} \right] \delta z ds - \mathcal{H} \Delta s|_{s_1}^{s_2} + \left. \frac{\partial \mathcal{L}}{\partial \psi_s} \Delta \psi \right|_{s_1}^{s_2} \\ & + \left. \frac{\partial \mathcal{L}}{\partial r_s} \Delta r \right|_{s_1}^{s_2} + \left. \frac{\partial \mathcal{L}}{\partial z_s} \Delta z \right|_{s_1}^{s_2} - \frac{F}{2\pi\kappa} \Delta z|_{s_1}, \end{aligned} \quad (2.5)$$

where $\delta E'_{\mathcal{L}} = 0$ gives a stationary shape, and variations of each coordinate at the poles are given by

$$\Delta r = \delta r + r_s \Delta s, \quad \Delta z = \delta z + z_s \Delta s, \quad \Delta \psi = \delta \psi + \psi_s \Delta s, \quad (2.6)$$

according to (4.5). In Eq. (2.5), $\mathcal{H} \equiv \mathcal{L} - \psi_s \partial \mathcal{L} / \partial \psi_s - r_s \partial \mathcal{L} / \partial r_s - z_s \partial \mathcal{L} / \partial z_s$ plays the role of the Hamiltonian of the system

$$\mathcal{H} = \frac{r}{2} \left[\psi_s^2 - \left(\frac{\sin \psi}{r} \right)^2 \right] - \frac{\Sigma}{\kappa} r - \frac{1}{2} \frac{P}{\kappa} r^2 \sin \psi + \gamma \cos \psi - \eta \sin \psi, \quad (2.7)$$

as defined in Eq. (4.7) in section 4. Given that the Langrangian function (2.3) is not an explicit function of arclength, i.e. $\frac{\partial \mathcal{L}}{\partial s} = 0$, then

$$\frac{d\mathcal{H}}{ds} = 0 \quad (2.8)$$

and \mathcal{H} is constant.

When $\delta G'_{\mathcal{L}} = 0$, the terms in the integrand of Eq. (2.5) yield a system of Euler-Lagrange shape equations for arbitrary variations of (r, z, ψ) as follows,

$$\psi_{ss} = \frac{\cos \psi \sin \psi}{r^2} - \frac{\psi_s}{r} \cos \psi + \frac{1}{2} \frac{P}{\kappa} r \cos \psi + \frac{\gamma}{r} \sin \psi + \frac{\eta}{r} \cos \psi, \quad (2.9)$$

$$\gamma_s = \frac{1}{2} \psi_s^2 - \frac{\sin^2 \psi}{2r^2} + \frac{\Sigma}{\kappa} + \frac{P}{\kappa} r \sin \psi, \quad (2.10)$$

$$\eta_s = 0, \quad (2.11)$$

where the Lagrange multiplier functions γ and η enforce the geometric arclength relations (2.1) locally.

Boundary conditions (12)-(13) in the main text still apply for the system of equations (2.9)-(2.11). Note that Eq. (13) combined with the arclength relation (11) and the radial geometric constraint (i.e., $r_s = \cos \psi$) yield equivalent boundary conditions for the tilt angle,

$$\psi(0) = 0, \quad \psi(L) = \pi, \quad (2.12)$$

which enforce that the first three terms and the last term in Eq. (2.7) vanish, leading to

$$\gamma(0) = \gamma(L) = \mathcal{H}, \quad (2.13)$$

where,

$$\mathcal{H} \equiv 0, \quad (2.14)$$

for arbitrary variations in arclength at the poles.

Constraints of constant area and constant volume can be imposed globally using

$$A_T - \int_0^L 2\pi r ds = 0, \quad (2.15)$$

and

$$V_T - \int_0^L \pi r^2 \sin \psi ds = 0. \quad (2.16)$$

Equation (2.14) implies that the meridional, pole-to-pole distance L of the vesicle is determined self-consistently (i.e., for $\Delta s|_{poles} \neq 0$) to satisfy the extremum condition on the elastic energy, $\delta E'_{\mathcal{L}} = 0$. Moreover, boundary conditions of fixed angles at the poles and closed vesicle shapes yield $\Delta \psi|_{poles} = \Delta r|_{poles} = 0$, respectively. For non-zero changes in height of the vesicle, $\Delta z|_{s_1} \neq 0$, a point force of the form shown in Eq. (23) in the main text is needed to enforce

$\delta E'_L = 0$, where we assumed, by symmetry, that the forces acting on both poles are equal and point in opposite directions. The same relation for the force given by Eq. (23) is recovered in section 3 using the local behavior of the tilt angle (3.7), the extremum of the energy Eq. (6), and the definition of the axial force (7) in the main text.

The system of Euler-Lagrange equations (2.9)-(2.11) and boundary conditions (12) in the main text, (2.12), (2.13), and (2.14) along with the geometric relations (2.1), (2.15) and (2.16) can be solved numerically for axisymmetric vesicle shapes. A possible numerical approach is to use an implicitly, two-point boundary value problem in a truncated domain with modified boundary conditions to avoid coordinate singularities at the poles [5]. This analysis can be conducted for an ensemble of axisymmetric membranes with edges (or holes at both poles) held at a fixed separation by an axial force, where the same form of Eq. (23) in the main text has been derived in Ref. [6].

In the constant-height scenario, the potential (2.2) is modified using relation (23) in the main text directly, [7, 8]

$$\tilde{G}' = 2\pi\kappa \int_{s_1}^{s_2} \tilde{\mathcal{L}}(r, r_s, \psi, \psi_s) ds, \quad (2.17)$$

where the axial force appears in the modified Lagrangian and enforces the geometrical constraint of constant height as follows

$$\tilde{\mathcal{L}} = \frac{r}{2} \left(\psi_s + \frac{\sin \psi}{r} \right)^2 + \frac{\Sigma}{\kappa} r + \frac{1}{2} \frac{P}{\kappa} r^2 \sin \psi + \gamma(r_s - \cos \psi) + \frac{F}{2\pi\kappa} \sin \psi, \quad (2.18)$$

and

$$h_0 + \int_0^L \sin \psi ds = 0, \quad (2.19)$$

enforces a relation for the fixed height, h_0 , using $z_s = -\sin \psi$. Taking the first variation of (2.17) following the steps used in the energy minimization of Eq. (2.5), yields a system of Euler-Lagrange equations dynamically equivalent to (2.9)-(2.10) where one uses Eq. (23) in the main text to eliminate η . In this case, the boundary conditions are $r(0) = r(L) = 0$, $z(0) = 0$ and $z(L) = h_0$ with the geometric constraints on area, volume, and height given by (2.15), (2.16), and (2.19), respectively. The boundary terms in the energy minimization (cf. Eq. (2.5)) yield the addition condition $\tilde{\mathcal{H}} \equiv 0$ for $\Delta s|_{poles} \neq 0$, where

$$\tilde{\mathcal{H}} = \frac{r}{2} \left[\psi_s^2 - \left(\frac{\sin \psi}{r} \right)^2 \right] - \frac{\Sigma}{\kappa} r - \frac{1}{2} \frac{P}{\kappa} r^2 \sin \psi + \gamma \cos \psi - \frac{F}{2\pi\kappa} \sin \psi, \quad (2.20)$$

by definition $\tilde{\mathcal{H}} \equiv \tilde{\mathcal{L}} - \psi_s \partial \tilde{\mathcal{L}} / \partial \psi_s - r_s \partial \tilde{\mathcal{L}} / \partial r_s$, and the condition of zero moment at the poles

$$(r\psi_s + \sin \psi)|_{poles} = 0, \quad (2.21)$$

for $\Delta \psi|_{poles} \neq 0$. The numerical solution of the modified system of Euler-Lagrange equations determines the pressure, tension, and axial force for specified values of volume, area, and height, respectively; the length L and the tilt-angle at the poles are determined self-consistently such that $\tilde{\mathcal{H}}$ is constant and the moment is zero.

2.1 Note on the correspondence between shape equations

The direct correspondence between the general shape equation (8) in the main text and Eqs. (2.9)-(2.11) is obtained by eliminating the Lagrange multiplier functions (γ, η) from Eqs. (2.9)-(2.11) and (2.7) using $\mathcal{H} \equiv 0$.

The steps are as follows: (i) eliminate $\eta = \eta(\psi, \psi_s, r, \gamma)$ from Eq. (2.7) setting $\mathcal{H} = 0$; (ii) this expression is then used in Eq. (2.9) to yield a relation for $\gamma = \gamma(\psi, \psi_s, \psi_{ss}, r)$; (iii) finally, γ is eliminated from Eq. (2.10) by differentiation with respect to arclength. This procedure results in a third-order shape equation in the tilt angle as previously reported in the literature [4], that can be recast in the form of Eq. (8) using definitions (9)-(10) and relation (2) in the main text.

This equivalence between the general form of the shape equation (8) in the main text and the system of Euler-Lagrange equations for axisymmetric vesicle shapes was a controversial topic in the 90s and early 2000s [4,9–13]. Ou-Yang and coworkers [9,10] argued that the Euler-Lagrange shape equations when parametrized by the radial distance from the symmetry axis to a point on the surface [14,15], or by arclength [3] led to different shape equations when compared to the general shape equation (8) specialized to axisymmetric geometries. Zheng & Liu [11] showed that both shape equations (see Eqs.(2) and (3) in Ref. [11]) are related by a simple formula where the Euler-Lagrange shape equation is cast as a first integral of the more general, higher-order shape equation. In fact, both equations yield the same results for closed vesicles with smooth profiles where the constant of integration in Eq.(5) of Ref. [11] is set to zero. This constant of integration can be associated with the axial point force discussed above [7,8] and hence vesicles with smooth, analytical contours are freely suspended or unconstrained. In this limit, vesicle contours are independent of the choice of parametrization, the total length and the height of the vesicle are free to vary, and the resulting vesicle profiles reduce to a special subset of minimum energy, stationary solutions to Eq. (8) [7]. The complementary, higher-energy set of vesicle shapes obtained from Eq. (8) lose analyticity at the poles where discontinuities in higher order derivatives of space variables are predicted [8,12]. These non-analytic stationary shapes are associated with vesicle configurations resulting from the action of axial point forces, or, equivalently from an additional geometric constraint of fixed vesicle height [4,12,16].

Blyth & Pozrikidis [13] revisited this topic and pointed out inconsistencies in the derivation of the Euler-Lagrange shape equations (2.9)-(2.11) with $\eta = 0$ when the “Hamiltonian” function of this system is set to zero. The authors presented numerical solutions to the general shape equation (8) for axisymmetric shapes and enforced smoothness of the profile at the poles by setting $dc_1/ds = 0$ as one of the boundary conditions. Note that this is equivalent to setting the axial point force to zero (cf. Eq. (7)) which yields a special subset of stationary solutions to Eq. (8). Hence, the results shown in Figs. 3(a)-(c) of Blyth & Pozrikidis are for freely suspended vesicles and are in agreement with the results obtained from the system of Euler-Lagrange shape equations reported in Refs. [3,4] with $\eta = 0$.

Blyth & Pozrikidis [13] also computed axisymmetric shapes using a thin-shell formulation for isotropic tensions and isotropic stress resultants integrated across the membrane thickness. Their results indicate a broader set of stationary shapes that arise from the solution of stress balance shape equations that are dynamically-equivalent, not exactly equal to Eq. (8) in the main text or Eq. 3 in Ref. [13]. The reason for this difference in form of the shape equations is a consequence of the choice of the linear constitutive equation for the meridional, M_m , and azimuthal, M_ϕ , bending moments acting on a patch of membrane. For instance, for $M_m = \kappa c_1$ and $M_\phi = \kappa c_2$, where κ is the bending rigidity, the shape equations derived from force-torque balance assuming isotropic lateral tensions and isotropic integrated stresses derived in Ref. [13] differ from the shape equation (8); however, as shown in the Appendix of Powers et al. [17], the general shape equation is recovered if the bending moments are defined in terms of the mean curvature, i.e., $M_m = M_\phi = \kappa(c_1 + c_2)$.

Some vesicle profiles reported in Ref. [13] are in qualitative agreement with the solutions shown in section 3 of the main text; however, self-intersection of the shapes in multi-lobed

branches or pinching dynamics at the poles of vesicles with elongated tips are not verified in our work for vesicle shapes with two-fold symmetry. This suggests that the physical conditions in both works are different within a higher dimensional configurational space; moreover, all numerical solutions in Ref. [13] are for unconstrained vesicles.

3 Local analysis of the shape equation near the poles

In this section we show a local analysis of the tilt angle near the pole (i.e., for $|s| \ll 1$) where we take $\psi \rightarrow 0$ and $r \rightarrow 0$. Since $r_s = 1$ at $s = 0$, it follows from Eq. (2.1) that $r \sim s$ to leading order. In this limit, Eq. (2.10) reduces to

$$\gamma_s \sim \frac{\Sigma}{\kappa} + \frac{1}{2} \left[\psi_s^2 - \frac{\psi^2}{r^2} \right]. \quad (3.1)$$

Since $\mathcal{H} \equiv 0$, we assume $r \left[\psi_s^2 - \frac{\psi^2}{r^2} \right] \rightarrow 0$ as $s \rightarrow 0$ yielding a linear, local behavior for the Lagrange multiplier function,

$$\gamma \sim \frac{\Sigma}{\kappa} s, \quad (3.2)$$

implying that $\gamma(0) = 0$. Inspection of Eq. (2.9) in the limit as $|s| \ll 1$, leads to

$$\psi_{ss} \sim \left(\frac{\psi}{s^2} - \frac{\psi_s}{s} + \frac{\eta}{s} \right) + \frac{1}{2} \frac{P}{\kappa} s + \frac{\gamma \psi}{s}. \quad (3.3)$$

Since both γ and ψ tend to zero as $s \rightarrow 0$, we neglect the term $\sim (\gamma\psi)/s$; note that the pressure term also vanishes as $s \rightarrow 0$. Thus, to leading order, the tilt-angle is governed by

$$s^2 \psi_{ss} + s \psi_s - \psi = -\eta s, \quad (3.4)$$

that admits a homogeneous solution of the form,

$$\psi \sim a s + \frac{b}{s}, \quad (3.5)$$

where we set $b = 0$ since $\psi \rightarrow 0$ as $s \rightarrow 0$. A particular solution to Eq. (3.4) is

$$\psi_p = -\frac{1}{2} \eta s \ln s, \quad (3.6)$$

and hence the general solution local to $s = 0$ is

$$\psi \sim a s - \frac{1}{2} \eta s \ln s. \quad (3.7)$$

An equivalent local form for the tilt angle ψ has been previously reported in Ref. [7]. Inserting the local behavior for the tilt angle (3.7) into Eq. (3.4) confirms, after integration, the leading order behavior of γ given by Eq. (3.2) using $\gamma(0) = 0$. In fact,

$$\gamma \sim \gamma_0 s + \gamma_1 s \ln s \quad (3.8)$$

where

$$\gamma_0 = \frac{\Sigma}{\kappa} - \frac{\eta}{2} \left(a + \frac{\eta}{4} \right), \quad (3.9)$$

and

$$\gamma_1 = \frac{\eta^2}{4}. \quad (3.10)$$

The local behavior for the spatial variables (r, z) can be obtained directly from the local behavior of the tilt angle ψ . Inserting Eq. (3.7) into relations (2.1), one gets after integration

$$r \sim s + r_1 s^3 (\ln s)^2 + r_2 s^3 \ln s + r_3 s^3 + O(s^5 (\ln s)^4), \quad (3.11)$$

and

$$z \sim h_0 + z_1 s^2 \log s + z_2 s^2 + O(s^4 (\ln s)^3), \quad (3.12)$$

where the $O(1)$ constant of integration in Eq. (3.11) is set to zero for closed shapes, h_0 is the height of the vesicle at $s = 0$ (north pole) and the south pole is located at the origin of the coordinate system illustrated in Fig. 1(b) of the main text (i.e., $z(s_2) = 0$). The asymptotic coefficients in Eqs. (3.11) and (3.12) are

$$r_1 = -\frac{1}{24}\eta^2, \quad r_2 = \eta \left(\frac{a}{6} + \frac{\eta}{36} \right), \quad r_3 = -\frac{a}{6} - \eta \left(\frac{a}{18} + \frac{\eta}{108} \right), \quad (3.13)$$

and

$$z_1 = \frac{\eta}{4}, \quad z_2 = -\left(\frac{a}{2} + \frac{\eta}{8} \right), \quad (3.14)$$

respectively.

Equations (3.11)-(3.12) show non-analytic behavior for the spatial variables (r, z) near the poles. If $\eta = 0$, r and z can be expressed as Taylor series expansions of cosine and sine about $s = 0$, respectively, since $\psi \sim as \rightarrow 0$ as $s \rightarrow 0$ and the logarithmic dependence is removed. In this case, the contours are considered smooth for all s .

A direct relation between the Lagrange multiplier η and the axial force, F , is obtained using definition (7) in the main text and the asymptotic behavior of the tilt angle (3.7), yielding Eq. (23), where $H_s \sim \psi_{ss}$ and $r \sim s$. Smooth vesicle contours with local analytic behavior for $|s| \ll 1$ implies that the axial force vanishes at the poles (i.e., the vesicle is freely suspended) if, and only if, $H_s = 0$. Alternatively, if the Lagrange multiplier η is nonzero and finite, the point-force acting at the poles is also nonzero and finite since $(H_s r)|_{poles}$ is bounded for shapes with finite energy. The non-analyticity of axisymmetric, closed contours when $\eta \neq 0$ has been pointed out in the literature in Refs. [4, 12]. Note that the local behavior of ψ leading to $\gamma(0) = 0$ implies that the ‘‘Hamiltonian’’ of the system is constant and equal to zero for all s even when η is nonzero and finite. In this case, the axial force is sufficient to guarantee the interfacial force balance (8) at the poles or, equivalently, to satisfy the condition that the first variation of the total elastic energy (6) is zero for all s (cf. Eq. (2.5)).

3.1 Effect of spontaneous curvature

The local analysis presented in section 3 can be extended to include the effect of spontaneous curvature, where the shape equations (2.9) and (2.11) remain the same, and Eq. (2.10) becomes [4]

$$\gamma_s = \frac{1}{2}(\psi_s - C_0)^2 - \frac{\sin^2 \psi}{2r^2} + \frac{\Sigma}{\kappa} + \frac{P}{\kappa} r \sin \psi. \quad (3.15)$$

Inserting the rescaled forms of the tilt angle and tension

$$\tilde{\psi} = \psi - C_0 r, \quad (3.16)$$

and

$$\tilde{\Sigma} = \Sigma - \frac{1}{2}\kappa C_0^2, \quad (3.17)$$

in Eq. (3.15) yields

$$\gamma_s \sim \frac{\tilde{\Sigma}}{\kappa} - \frac{\tilde{\psi}}{r} C_0 + \frac{1}{2} \left[\tilde{\psi}_s^2 - \frac{\tilde{\psi}^2}{r^2} \right]. \quad (3.18)$$

We follow assumption (3.2) where

$$\gamma \sim \frac{\tilde{\Sigma}}{\kappa} s, \quad (3.19)$$

is obtained by inspection of the Hamiltonian Eq. (2.7) using the condition $\mathcal{H} \equiv 0$ given that

$$r \left[\tilde{\psi}_s^2 - \frac{\tilde{\psi}^2}{r^2} \right] \rightarrow 0, \quad (3.20)$$

$$\gamma \sim r \tilde{\psi}_s C_0, \quad (3.21)$$

and $\gamma(0) = 0$. Hence, the governing equation for the rescaled tilt angle $\tilde{\psi}$ has the same form as in Eq. (3.4) with solution given by

$$\tilde{\psi} \sim a s - \frac{1}{2} \eta s \ln s, \quad (3.22)$$

where assumptions (3.20)-(3.21) are automatically satisfied. Substituting the rescaled solution for $\tilde{\psi}$ into Eq. (3.18) yields the local behavior

$$\gamma \sim \tilde{\gamma}_0 s + \gamma_1 s \ln s + O(s^2 \ln s) \quad (3.23)$$

where

$$\tilde{\gamma}_0 = \frac{\tilde{\Sigma}}{\kappa} - \frac{\eta}{2} \left(a + \frac{\eta}{4} \right), \quad (3.24)$$

and γ_1 is given by Eq. (3.10).

4 Hamilton's Principle of Stationary Action

In this section we present a derivation of Hamilton's principle of stationary action following [18] to complement the discussion on the tilt-angle formulation for stationary shapes presented in section 2. Hamilton's principle of stationary action is typically associated with the minimum of an action functional defined as

$$S = \int_{t_i}^{t_f} \mathcal{L}(\mathbf{q}(t), \dot{\mathbf{q}}(t), t) dt, \quad (4.1)$$

where \mathcal{L} is the Lagrangian of a system in a configurational space spanned by n generalized coordinates \mathbf{q} and velocities $\dot{\mathbf{q}}$. Let the scalar action S represent the extremum path between initial and final states of a system at two different times t_i and t_f , respectively. Taking the variation of S by sampling through a family of neighbouring paths defined at $t_i \rightarrow t_i + \Delta t_i$, $t_f \rightarrow t_f + \Delta t_f$, and $q_j(t) \rightarrow q_j(t) + \delta q_j(t)$, where δ represents an infinitesimal virtual displacement, yields the incremental change in the action

$$\delta S = \int_{t_i}^{t_f} \sum_j \left(\frac{\partial \mathcal{L}}{\partial q_j} \delta q_j + \frac{\partial \mathcal{L}}{\partial \dot{q}_j} \delta \dot{q}_j \right) dt + [\mathcal{L} \Delta t]_{t_i}^{t_f}, \quad (4.2)$$

where $j = 1, \dots, n$ spans the space of generalized coordinates and velocities. Integrating by parts the second term in the sum of Eq. (4.2), results in

$$\delta S = \int_{t_i}^{t_f} \sum_j \left(\frac{\partial \mathcal{L}}{\partial q_j} - \frac{d}{ds} \frac{\partial \mathcal{L}}{\partial \dot{q}_j} \right) \delta q_j dt + \left[\mathcal{L} \Delta t - \sum_j \frac{\partial \mathcal{L}}{\partial \dot{q}_j} \delta q_j \right]_{t_i}^{t_f}. \quad (4.3)$$

Equation (4.3) includes the variation of the Lagrangian along the path, and additional variations at the endpoints including the effect of increments in time between neighbouring paths.

The stationary principle in Lagrangian mechanics is centered on the determination of extremum paths undertaken by a system between two fixed locations in configurational space at two different times (e.g., $\mathbf{q}_j(t_i)$ and $\mathbf{q}_j(t_f)$). The end coordinate points are fixed and hence $\delta q_j(t_i) = \delta q_j(t_f) = 0$ and $\Delta t_i = \Delta t_f = 0$; in this limit, Eq.(4.3) simplifies to

$$\delta \tilde{S} = \int_{t_i}^{t_f} \sum_j \left(\frac{\partial \mathcal{L}}{\partial q_j} - \frac{d}{ds} \frac{\partial \mathcal{L}}{\partial \dot{q}_j} \right) \delta q_j dt, \quad (4.4)$$

where, for independent variations of the generalized coordinates, the term in parenthesis vanishes yielding a stationary path (i.e., $\delta \tilde{S} = 0$) along which the system evolves in time according to the Euler-Lagrange equations.

The stationary principle in Hamiltonian mechanics, involves the general variation of the Lagrangian functional as shown in (4.3), where the relative action between two paths is taken at different initial and final locations at different initial and final times. The integral term in (4.3) vanishes yielding a set Euler-Lagrange equations for the system, and the remaining term contains endpoint contributions to the variation. Let the total variation at each endpoint be defined as

$$\Delta q_j = \delta q_j + \dot{q}_j \Delta t; \quad (4.5)$$

inserting (4.5) into the second term on the right-hand-side of Eq. (4.3) results in

$$\delta S = \left[\sum_j \frac{\partial \mathcal{L}}{\partial \dot{q}_j} \Delta q_j - \mathcal{H} \Delta t \right]_{t_i}^{t_f}, \quad (4.6)$$

where

$$\mathcal{H} \equiv -\mathcal{L} + \sum_j \frac{\partial \mathcal{L}}{\partial \dot{q}_j} \dot{q}_j, \quad (4.7)$$

is the Hamiltonian of the system, and Eq.(4.7) represents Hamilton's principle of least action.

5 Experimental methods

5.1 Detailed balance analysis

To check for the equilibrium nature of the fluctuations, we tested for broken detailed balance in the transitions between microscopic configurations based on height-height membrane fluctuations [19] (see chapter 6 of Ref. [20] for more details about the method). The configurations correspond to the shapes defined by different Fourier modes. In equilibrium, it is equally likely for the forward and backward transitions to occur between any two different Fourier modes. A non-equilibrium system, however, would display a probability flux in the phase space of shapes. Figure 2 shows the probability density map for Fourier modes 3 and 4 of vesicles fluctuations

in the absence and presence of electric field strength, as indicated. The probability is defined as the ratio of the time spent at a given state. The arrows indicate the currents across box boundaries determined by counting transitions between boxes. A nonzero value of the contour integral of the probability current, $\Omega = \frac{\oint_C \mathbf{j} \cdot d\mathbf{l}}{\oint_C |\mathbf{j}| dl}$, would indicate out of equilibrium dynamics. However, we noticed for moderate electric field strength ranging from 0-10 kV/m the detailed balance was not broken as indicated by $\Omega \sim 0$. This implies that the fluctuations are still thermally driven in the presence of electric field.

We characterized the Gaussianity of the fluctuations using the fourth PDF moment, Kurtosis, Kurt. For a Gaussian distribution, Kurt = 3. In Figure 2 we demonstrated the Kurtosis for every mode number for the same vesicle in presence (7 kV/m) and absence of electric field strength. Our results confirm the previous analysis of unbroken Detailed balance with Kurtosis values Kurt \sim 3 for membrane fluctuations in the presence of electric field as well.

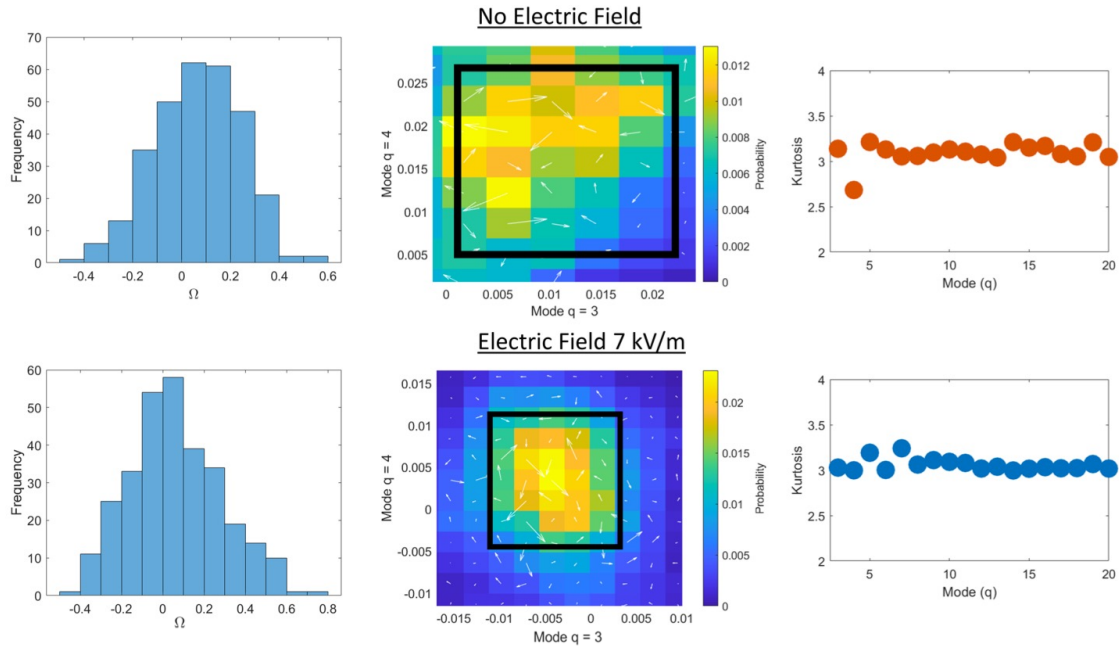


Figure 2: Nature of membrane fluctuations probed in the presence and absence of electric field. Probability current flux, Ω , detailed balance, and Kurtosis values for DOPC vesicle in the absence of applied field strength (a), and in the presence of electric field at 7 kV/m, (b). The salt concentration in the inner and outer solutions for DOPC vesicles are 0.4 mM NaCl and 0.8 mM NaCl, respectively.

References

- [1] Dirk Jan Struik. *Lectures on classical differential geometry*. Courier Corporation, 1961.
- [2] Udo Seifert. Configurations of fluid membranes and vesicles. *Advances in Physics*, 46(1):13–137, 1997.
- [3] Udo Seifert, Karin Berndl, and Reinhard Lipowsky. Shape transformations of vesicles: Phase diagram for spontaneous- curvature and bilayer-coupling models. *Phys. Rev. A*, 44:1182–1202, Jul 1991.

- [4] Frank Jülicher and Udo Seifert. Shape equations for axisymmetric vesicles: A clarification. *Phys. Rev. E*, 49:4728–4731, May 1994.
- [5] Hongyuan Jiang, Greg Huber, Robert A Pelcovits, and Thomas R Powers. Vesicle shape, molecular tilt, and the suppression of necks. *Physical Review E*, 76(3):031908, 2007.
- [6] Leroy L Jia, Steven Pei, Robert A Pelcovits, and Thomas R Powers. Axisymmetric membranes with edges under external force: buckling, minimal surfaces, and tethers. *Soft Matter*, 17(31):7268–7286, 2021.
- [7] Bojan Bozic, Sasa Svetina, and Bostjan Zeks. Theoretical analysis of the formation of membrane microtubes on axially strained vesicles. *Physical Review E*, 55(5):5834, 1997.
- [8] Imre Derényi, Frank Jülicher, and Jacques Prost. Formation and interaction of membrane tubes. *Physical review letters*, 88(23):238101, 2002.
- [9] Hu Jian-Guo and Ou-Yang Zhong-Can. Shape equations of the axisymmetric vesicles. *Physical Review E*, 47(1):461, 1993.
- [10] Hiroyoshi Naito, Masahiro Okuda, and Ou-Yang Zhong-Can. Counterexample to some shape equations for axisymmetric vesicles. *Physical Review E*, 48(3):2304, 1993.
- [11] Wei-Mou Zheng and Jixing Liu. Helfrich shape equation for axisymmetric vesicles as a first integral. *Phys. Rev. E*, 48:2856–2860, Oct 1993.
- [12] Rudolf Podgornik, Saša Svetina, and Boštjan Žekš. Parametrization invariance and shape equations of elastic axisymmetric vesicles. *Physical Review E*, 51(1):544, 1995.
- [13] MG Blyth and C Pozrikidis. Solution space of axisymmetric capsules enclosed by elastic membranes. *European Journal of Mechanics-A/Solids*, 23(5):877–892, 2004.
- [14] HJ Deuling and W Helfrich. The curvature elasticity of fluid membranes: a catalogue of vesicle shapes. *Journal de Physique*, 37(11):1335–1345, 1976.
- [15] Saša Svetina and Boštjan Žekš. Membrane bending energy and shape determination of phospholipid vesicles and red blood cells. *European biophysics journal*, 17(2):101–111, 1989.
- [16] Jemal Guven and Pablo Vázquez-Montejo. The geometry of fluid membranes: Variational principles, symmetries and conservation laws. In *The Role of Mechanics in the Study of Lipid Bilayers*, pages 167–219. Springer, 2018.
- [17] Thomas R. Powers, Greg Huber, and Raymond E. Goldstein. Fluid-membrane tethers: Minimal surfaces and elastic boundary layers. *Phys. Rev. E*, 65:041901, Mar 2002.
- [18] Douglas Cline. *Variational principles in classical mechanics*. University of Rochester River Campus Librarie, 2017.
- [19] Christopher Battle, Chase P Broedersz, Nikta Fakhri, Veikko F Geyer, Jonathon Howard, Christoph F Schmidt, and Fred C MacKintosh. Broken detailed balance at mesoscopic scales in active biological systems. *Science*, 352(6285):604–607, 2016.
- [20] H A Faizi. *Mechanical Characterization of Biomimetic Membranes Based on Fluctuation Spectroscopy and Electrodeformation*. Northwestern University, 2022.